Orbital Contributions to the Electron g Factor in Semiconductor Nanowires

Georg W. Winkler,[1,*] Dániel Varjas,[2] Rafal Skolasinski,[2] Alexey A. Soluyanov,[1,3] Matthias Troyer,[1,4] and Michael Wimmer[2]
[1]Theoretical Physics and Station Q Zurich, ETH Zurich, 8093 Zurich, Switzerland
[2]QuTech and Kavli Institute of Nanoscience, Delft University of Technology, 2600 GA Delft, Netherlands
[3]Department of Physics, Saint Petersburg State University, Saint Petersburg 199034, Russia
[4]Quantum Architectures and Computation Group, Microsoft Research, Redmond, Washington 98052, USA
(Received 30 March 2017; published 21 July 2017)

Recent experiments on Majorana fermions in semiconductor nanowires [S. M. Albrecht, A. P. Higginbotham, M. Madsen, F. Kuemmeth, T. S. Jespersen, J. Nygård, P. Krogstrup, and C. M. Marcus, Nature (London) **531**, 206 (2016)] revealed a surprisingly large electronic Landé g factor, several times larger than the bulk value—contrary to the expectation that confinement reduces the g factor. Here we assess the role of orbital contributions to the electron g factor in nanowires and quantum dots. We show that an $\mathbf{L}\cdot\mathbf{S}$ coupling in higher subbands leads to an enhancement of the g factor of an order of magnitude or more for small effective mass semiconductors. We validate our theoretical finding with simulations of InAs and InSb, showing that the effect persists even if cylindrical symmetry is broken. A huge anisotropy of the enhanced g factors under magnetic field rotation allows for a straightforward experimental test of this theory.

DOI: 10.1103/PhysRevLett.119.037701

Early electron spin resonance experiments in the two-dimensional electron gas (2DEG) formed in AlGaAs/GaAs heterostructures found a reduced Landé g factor of electrons [1], which was later theoretically explained to arise due to the electronic confinement [2–4]. It is by now well established that confinement in a nanostructure leads to a reduction in the g factor [5,6]—the subband confinement increases the energy gap, which is inversely proportional to $g^* - g_0$, where g^* is the effective and g_0 the free electron g factor [5,8]. Surprisingly, experiments in InAs [9,10] and InSb [11,12] nanowires found g factors surpassing the corresponding bulk g factors by up to 40%.

Recently, this discrepancy has attracted interest due to the experimental discovery of a zero bias conductance peak in semiconductor nanowires' proximity coupled to an s-wave superconductor [13–17], which is believed to be a signature of the Majorana bound state [18–20] having possible applications in topological quantum computation [21,22]. The electron g factor of the semiconductor nanowire determines the strength of magnetic field required to trigger the topological phase transition in these systems. It is desirable to keep the magnetic field low since it also suppresses superconductivity, and thus a large g-factor semiconductor is desired. Furthermore, Majorana proposals based on magnetic textures [23–25] and various spintronic devices [26] require large g factors. Small band-gap semiconductors like InAs and InSb are therefore the materials of choice for Majorana nanowires, having large g factors and strong spin-orbit coupling (SOC).

In a recent experiment with InAs nanowires g factors [27] more than three times larger than the bulk g factor ($g^*_{\mathrm{InAs}} = -14.9$ [5,28]) were measured [16]. Moreover, it was found that the g factor depends very strongly on the chemical potential μ tuned by the gate potential [29]. For low μ small g factors were found, which can be explained by the bulk g factor of InAs. The anomalously large g factors have only been detected at high chemical potential μ.

In this work, we present a mechanism that can lead to very large g factors in higher subbands of nanowires and similarly shaped nanostructures. With this we can explain both the large g factors observed in Refs. [9–11,16], and the chemical potential dependence [29]. In particular, we find that the orbital angular momentum in the confined nanostructure plays a crucial role. The lowest conduction subband or state is characterized by no or only small orbital angular momentum. In this case the usual reasoning applies and confinement does lead to a reduction of the g factor. Higher subbands or states, however, can have nonzero orbital angular momentum in an approximately cylindrical structure. Because of strong SOC in small band-gap semiconductors one finds an $\mathbf{L}\cdot\mathbf{S}$-type spin alignment if the orbital angular momentum $\mathbf{L}$ is nonzero. Kramers pairs of opposite orbital angular momentum form at $B = 0$, and thus the g factor obtains an additional contribution resulting from the coupling of the orbital angular momentum to the magnetic field. A similar orbital enhancement of the g factor is known from the theory of the hydrogen atom [30] and has also been observed in carbon nanotubes [31,32]. However, due to the small effective mass the g-factor enhancement can be orders of magnitude larger in the semiconducting structures investigated here.

Cylindrical symmetry.—We start by considering cylindrical nanowires and estimate the maximally achievable g

factor for subbands as a function of their orbital angular momentum. Initially, we assume independent SU(2) spin rotation symmetry (no SOC) and time-reversal (TR) invariance without magnetic field. We then introduce a magnetic field parallel to the wire, thus preserving the rotational invariance (both in real space and spin) around the axis of the wire (z direction in the following).

As the wire is translationally invariant in the z direction, and the conduction band minimum is at $k_z = 0$, we restrict to $k_z = 0$ in the following and investigate the wave function in the xy plane only. As a consequence of separate real space and spin rotation symmetries, the states can be classified by their orbital angular momentum $L_z = 0$, $\pm\hbar$, $\pm 2\hbar$, etc. and spin $S_z = \pm(\hbar/2)$ (for brevity we drop the z subscript in the following and use the lowercase letters for angular momentum in units of $\hbar$). The lowest subband is twofold spin degenerate $|l = 0, s = \pm\frac{1}{2}\rangle$, higher subbands with $l \neq 0$ being fourfold $|\pm|l|, \pm\frac{1}{2}\rangle$.

In a simple quadratic band with an effective mass m^*, the momentum and electrical current are related as $\mathbf{J} = (e/m^*)\mathbf{p}$. Using the orbital angular momentum $\mathbf{L} = \mathbf{r} \times \mathbf{p}$ the orbital magnetic moment is expressible as

$$\mathbf{M}_o = \frac{1}{2}\mathbf{r} \times \mathbf{J} = -\frac{e}{2m^*}\mathbf{L} = -\frac{m_0}{m^*}\mu_B l \mathbf{e}_z. \tag{1}$$

We see that the orbital magnetic moment is enhanced by the low effective mass of the bands. Because of the fourfold degeneracy, we cannot unambiguously calculate g factors and thus next include spin-orbit coupling.

With SOC the orbital and spin angular momentum is no longer separately conserved, but the total angular momentum $f_z = l_z + s_z$ is still conserved and takes half-integer values. Without magnetic field the system is TR invariant. As angular momentum is odd under TR, the degenerate Kramers pairs have opposite f. Turning on SOC splits the fourfold degeneracy of the $l \neq 0$ subbands into two degenerate pairs: $|+|l|, +\frac{1}{2}\rangle$ and $|-|l|, -\frac{1}{2}\rangle$ stay degenerate [$f = \pm(|l| + \frac{1}{2})$] and so do $|+|l|, -\frac{1}{2}\rangle$ and $|-|l|, +\frac{1}{2}\rangle$ [$f = \pm(|l| - \frac{1}{2})$], as shown in Fig. 1(a). Even though the orbital and local angular momenta are no longer separately conserved their expectation values remain similar for realistic SOC strengths.

The magnetic field $\mathbf{B}$ couples to the total magnetic moment $\mathbf{M} = \mathbf{M}_o - g^*(e/2m_0)\mathbf{S}$ [4]. Using Eq. (1), the Zeeman splitting of a Kramer's pair $|\pm|l|, +\frac{1}{2}\rangle$ and $|\mp|l|, -\frac{1}{2}\rangle$ for a magnetic field in the z direction is given by $\Delta E_{\text{Zeeman}} = \mu_B[g^* \pm 2(m_0/m^*)|l|](B_z/2)$ and the resulting effective g factor can be read off,

$$g_{|l|\pm\frac{1}{2}} = g^* \pm 2\frac{m_0}{m^*}|l|. \tag{2}$$

Below we see from numerical simulation that this is a good approximation even in a less ideal case.

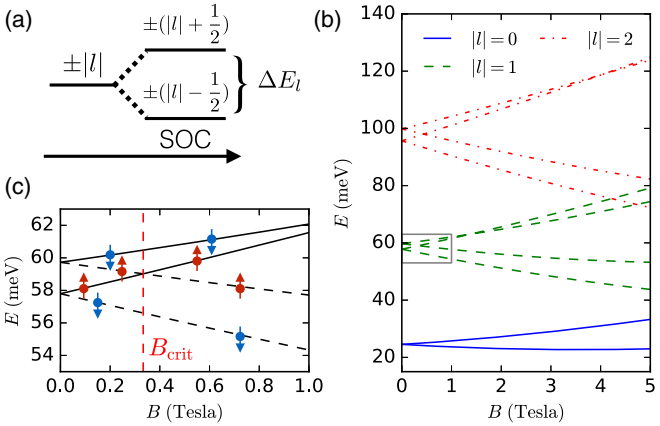

FIG. 1. (a) Evolution of the energy levels at $k_z = 0$ in cylindrical symmetry when SOC is turned on. (b) Energy levels of a cylindrical InSb wire with 40 nm diameter in an axial magnetic field. (c) Zoom in on the $|l| = 1$ states marked by the gray rectangle in (b). Dashed lines are $l = +1$, and solid lines $l = -1$, states. The spin alignments are marked by the small arrows and the vertical dashed red line marks B_{crit}.

This result is analogous to the well-known Landé g factor of the hydrogen atom when taking relativistic SOC into account: the splitting induced by weak external magnetic field has contributions from both the orbital and spin angular momentum [30]. This effect is amplified in semiconductor nanostructures because the small effective mass increases both the orbital magnetic moment and the bulk g factor g^*.

Wire simulations.—We next validate our theoretical findings with simulations of nanowires using an eight-band $\mathbf{k} \cdot \mathbf{p}$ model for zinc blende semiconductors [5,33,34]. At first, we assume perfect cylindrical symmetry of a nanowire, grown in the 001 direction, and employ the axial approximation [35–38]. In this case, the wave functions can be written as [49]

$$\psi(\rho, \phi, z) = \sum_n g_n(\rho, z) e^{i l_n \phi} |u_n\rangle, \tag{3}$$

where $|u_n\rangle$ are the basis states of the eight-band $\mathbf{k} \cdot \mathbf{p}$ Hamiltonian with local angular momentum j_n [50]. Since the Hamiltonian conserves the total angular momentum f one obtains the orbital part of each component as $l_n = f - j_n$. If we furthermore focus on an infinite wire in the z direction the problem is reduced to a one-dimensional boundary value problem in ρ that we solve using the finite difference method [38].

Figure 1(b) shows the subband edges of an InSb nanowire of 40 nm diameter. At $B = 0$ one generically finds the lowest conduction subband to originate from the $|l| = 0$ state without SOC. At higher energy there are the $|l| = 1$ and $|l| = 2$ states and then another $|l| = 0$ state with a higher radial quantum number (not shown). This order of states is generic as long as the conduction band is

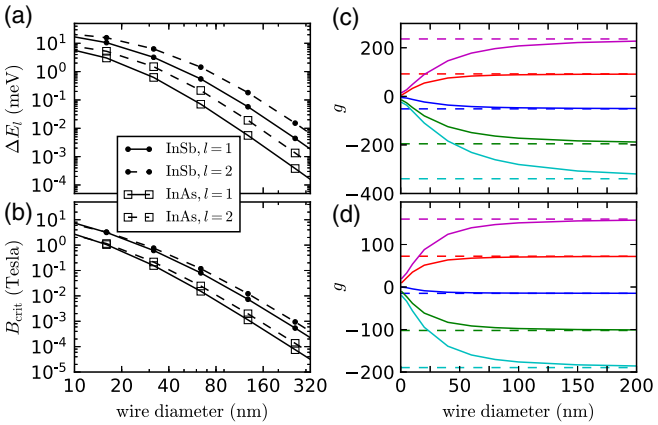

FIG. 2. (a) Diameter dependence of the SOC splitting ΔE_1 and ΔE_2 for InSb and InAs wires. (b) Diameter dependence of the critical magnetic field B_{crit} defined in Fig. 1(b). (c) [(d)] Effective g factors at infinitesimal magnetic field of the first five subbands of an InSb (InAs) wire: $l=0, |f|=\frac{1}{2}$ (blue), $|l|=1, |f|=\frac{1}{2}$ (green), $|l|=1, |f|=\frac{3}{2}$ (red), $|l|=2, |f|=\frac{3}{2}$ (cyan), and $|l|=2, |f|=\frac{5}{2}$ (magenta). The dashed lines in the corresponding colors are the prediction of Eq. (2) where we substituted bulk values.

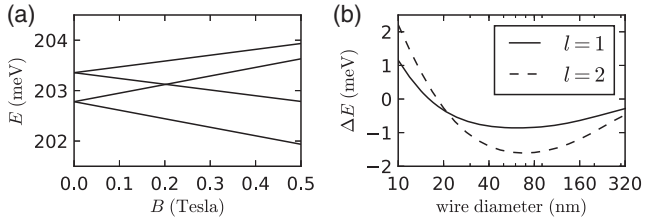

FIG. 3. (a) Energy levels of the lowest $|l|=1$ states as a function of B in a tight-binding simulation of a hexagonal InSb wire of 20.1 nm diameter, grown in the 111 direction. (b) SOC splitting as a function of diameter in a cylindrical wurtzite InAs wire.

approximately quadratic [51]. Figure 1(c) zooms in on the $|l|=1$ subbands. Because of SOC the $|f|=\frac{3}{2}$ and $|f|=\frac{1}{2}$ states are split at $B=0$ by $\Delta E_1 \approx 2$ meV. If a magnetic field $B < B_{\mathrm{crit}}$ [see Fig. 1(c)] is turned on a splitting between states of opposite orbital angular momentum l is observed and thus enhanced g factors according to Eq. (2). However, when the magnetic field is large, $B > B_{\mathrm{crit}}$, states of the same orbital angular momentum bundle together and their relative slope with respect to B corresponds to the normal g factor without orbital contributions. Thus a splitting ΔE_l is a crucial ingredient for enhanced g factors.

Figure 2 shows the dependence on the diameter of the nanowire. From the ΔE_l dependence it is evident that the wire cannot be made too thick to experimentally observe the effect with a detectable energy scale, e.g., to distinguish the split energy levels using Coulomb oscillations [52]. Figures 2(c) and 2(d) show that at large wire diameters Eq. (2) is reproduced perfectly by numerics, but for small diameters the g-factor enhancement is reduced by the confinement. Thus, the optimal diameter range where enhancement of the g factor is strong and at the same time ΔE_l and B_{crit} are large enough is in between 10 and 100 nm. We see that the g factors of higher subbands can be very large—enhancements of an order of magnitude compared to the bulk g factor are possible.

The splitting ΔE_l is generic if SOC is present, since in a typical semiconductor wire with SOC there is no symmetry that would protect the degeneracy between states of different total angular momentum. The conduction band of zinc blende semiconductors has a purely s-orbital character at the Γ point of the Brillouin zone, which is insensitive to SOC. Thus, also the conduction subbands of a zinc blende nanowire are mostly derived from s orbitals. Any nonzero splitting ΔE_l results from p-like hole contributions to the conduction band due to confinement. This explains why the splitting in the conduction band is so small compared to the split-off energy of the valence bands Δ, which is 0.81 eV for InSb and 0.38 eV for InAs [5].

Since ΔE_l results from the scattering of states at the surface of the wire, the boundary conditions impact the numerical value, and even the sign, of ΔE_l [38]. Abrupt boundaries can be problematic in $\mathbf{k}\cdot\mathbf{p}$ simulations [53]; therefore, we use tight-binding (TB) simulations to check the robustness of our results. The effective tight-binding Hamiltonian is generated from the first-principles s- and p-like Wannier functions [54], calculated using the Vienna *ab initio* simulation package (VASP) [55–58] with the projector augmented-wave method [59,60], a cut-off energy of 300 eV, a $8\times8\times8$ Monkhorst-Pack mesh, and using the HSE06 hybrid functional [61–63]. Furthermore, the TB model includes the Dresselhaus term that was neglected for the zinc blende $\mathbf{k}\cdot\mathbf{p}$ simulations since its effect is found to be very small [38]. In Fig. 3(a) we show the magnetic field dependence of the $|l|=1$ subbands in a hexagonal InSb wire. The g factors of -59 and $+40$ and $B_{\mathrm{crit}} \approx 0.2$ Tesla agree qualitatively with the $\mathbf{k}\cdot\mathbf{p}$ results.

While in zinc blende wires boundary effects are dominating, in wurtzite wires the situation is different: There, the conduction band has a mixed s and p character. Thus, wurtzite wires have an intrinsic splitting independent of confinement [64]. Using a $\mathbf{k}\cdot\mathbf{p}$ model for wurtzite semiconductors [65], we find a nearly size-independent ΔE_l of order 1 meV for [0001] grown wurtzite InAs wires for experimentally used diameters of 40 to 160 nm [66]; see Fig. 3(b). At very large wire diameters >200 nm the confinement induced subband splitting becomes smaller than ΔE_l, leading to a reduction of ΔE_l, and at very small diameters <20 nm the cubic Dresselhaus term dominates over the linear Rashba term, causing a sign change in ΔE_l [38,67].

Symmetry breaking.— We now consider the effects of broken cylindrical symmetry and solve the full two-dimensional cross section of hexagonal zinc blende wires,

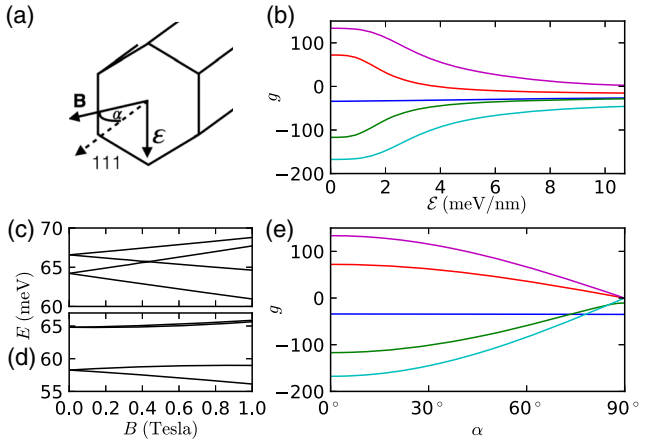

FIG. 4. (a) Magnetic and electric field directions in the hexagonal 111 wire. (b) The g factors measured at 0.2 Tesla ($\alpha = 0$) of a hexagonal InSb wire with 40 nm diameter as a function of a perpendicular electric field. (c) [(d)] Energy levels of the $|l| = 1$ states as a function of B at an electric field of $\mathcal{E} = 0$ meV/nm ($\mathcal{E} = 3$ meV/nm). (e) The g factors as a function of α measured at 0.2 Tesla in a hexagonal InSb wire with 40 nm diameter. In (b) and (e) the color code is the same as in Figs. 2(c) and 2(d).

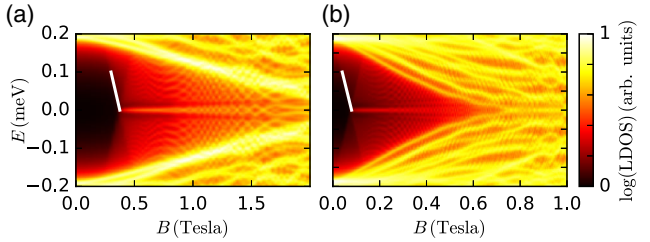

FIG. 5. (a) [(b)] shows the local density of states (LDOS) at the end of an InAs wire with 40 nm diameter and 2172 nm length in an electric field of $\mathcal{E} = 1.2$ meV/nm and proximity effect induced superconducting pairing $\Delta = 0.2$ meV. The chemical potential $\mu = 39.6$ meV ($\mu = 68.5$ meV) is tuned to the $|l| = 1$ ($|l| = 2$) subbands. The slope of the whites lines amounts to a g factor of 23 (43).

grown in the 111 direction, using a two-dimensional discretization of the $\mathbf{k} \cdot \mathbf{p}$ model [38,68]. We allow for symmetry breaking by electric field and off-axis magnetic field; see Fig. 4(a) for the definitions of the relevant directions. In experimental situations, the symmetry is generally broken by electric fields, e.g., due to the back gate for tuning the electron density in the wire [9,11,16,29]. We find that, especially in higher subbands, the enhanced g factors are quite robust to an external electric field.

In Figs. 4(b)–4(d) we simulate a hexagonal InSb wire, of 40 nm diameter, in a perpendicular external electric field $\mathcal{E}$. The point group of the wire at $\mathcal{E} = 0$ is C_{3v} and crossings between states of different angular momentum are protected, as illustrated in Fig. 4(c). At nonzero $\mathcal{E}$ the different angular momentum eigenstates hybridize, which reduces their orbital angular momentum expectation value. However, as shown in Figs. 4(b) and 4(d), the orbital contribution to the g factor remains very significant until very large fields are applied. Bands with larger values of $|l|$ have larger splitting ΔE_l and, therefore, the orbital contribution to their g factors is more robust and can remain significantly larger than the bulk g factor until large electric fields; e.g., see the cyan and magenta lines corresponding to $|l| = 2$ in Fig. 4(b).

The electron g-factor anisotropy in the magnetic field of 2DEGs is well established [3,5,69,70]. In our case of orbitally enhanced g factors in nanowires we expect an even stronger anisotropy. Indeed, the electron spins in subbands with $l \neq 0$ feel a very strong orbital magnetic field that aligns them (anti-) parallel to the wire axis. Therefore, a perpendicular magnetic field first needs to overcome this orbital effect to create a Zeeman splitting of the states [31,32].

This is illustrated in Fig. 4(e), where we simulate a hexagonal InSb wire of 40 nm diameter in a magnetic field of 0.2 Tesla. We show there the g factor as a function of the angle α between the magnetic field and the nanowire axis. While the g factor of the lowest $l = 0$ subband is unaffected by the direction of $\mathbf{B}$, the g factor for bands with $l \neq 0$ almost vanishes for perpendicular magnetic field. This strong anisotropy of the electron g factor can be used in experiments to prove the important role of orbital angular momentum in nanowires.

In a Majorana wire circular symmetry breaking by gate potentials and band bending is mandatory to create a Rashba effect in the wire [19,20,71]. The results shown above suggest that even in such an environment orbital effects still dominate the g factors of certain subbands in wires. This is illustrated in Figs. 5(a) and 5(b), where we simulate an InAs wire proximity coupled to an Al superconductor (see Supplemental Material [38] for the details of the simulation). When the chemical potential is tuned to the $|l| = 1$ and $|l| = 2$ subbands, the g factors, extracted from the slope of the Majorana state forming the Andreev bound state, are 23 and 43 [72], respectively. These g factors are significantly larger than the bulk g factor of InAs, thus reproducing the experimental result of Ref. [16].

Conclusions and Outlook.— In summary, we have provided a theory for the previously unexplained large g factors observed in nanowires. Our findings help to better understand and optimize Majorana experiments. Similar results apply to quantum dots. For cylindrical quantum dots we find that orbital g-factor enhancements are still significant if the length of the dot is much shorter than its diameter; see Supplemental Material [38] for more details. Because of the observed robustness of the effect, it also applies in irregularly shaped quantum dots and can explain g-factor fluctuations there.

We thank L. Kouwenhoven, S. Vaitiekėnas, M. T. Deng, C. M. Marcus, K. Ennslin, T. D. Stanescu, A. E. Antipov,

E. Rossi, and R. M. Lutchyn for useful discussions and Q. S. Wu for providing first-principles derived tight-binding models. This work was supported by Microsoft Research, the Netherlands Organization for Scientific Research (NWO), the Foundation for Fundamental Research on Matter (FOM), the European Research Council (ERC) through ERC Advanced Grant No. SIMCOFE, the Swiss National Science Foundation, and through the National Competence Centers in Research MARVEL and QSIT.

*winklerg@ethz.ch

[1] D. Stein, K. v. Klitzing, and G. Weimann, Phys. Rev. Lett. **51**, 130 (1983).
[2] G. Lommer, F. Malcher, and U. Rössler, Phys. Rev. B **32**, 6965 (1985).
[3] E. L. Ivchenko and A. A. Kiselev, Sov. Phys. Semicond. **26**, 827 (1992).
[4] A. A. Kiselev, E. L. Ivchenko, and U. Rössler, Phys. Rev. B **58**, 16353 (1998).
[5] R. Winkler, S. Papadakis, E. De Poortere, and M. Shayegan, *Spin-Orbit Coupling in Two-Dimensional Electron and Hole Systems* (Springer, New York, 2003), Vol. 41.
[6] With the exception of the exchange enhancement of g factors [7].
[7] T. Ando and Y. Uemura, J. Phys. Soc. Jpn. **37**, 1044 (1974).
[8] L. M. Roth, B. Lax, and S. Zwerdling, Phys. Rev. **114**, 90 (1959).
[9] S. Csonka, L. Hofstetter, F. Freitag, S. Oberholzer, C. Schönenberger, T. S. Jespersen, M. Aagesen, and J. Nygård, Nano Lett. **8**, 3932 (2008).
[10] M. D. Schroer, K. D. Petersson, M. Jung, and J. R. Petta, Phys. Rev. Lett. **107**, 176811 (2011).
[11] H. A. Nilsson, P. Caroff, C. Thelander, M. Larsson, J. B. Wagner, L.-E. Wernersson, L. Samuelson, and H. Q. Xu, Nano Lett. **9**, 3151 (2009).
[12] I. van Weperen, S. R. Plissard, E. P. A. M. Bakkers, S. M. Frolov, and L. P. Kouwenhoven, Nano Lett. **13**, 387 (2013).
[13] A. Das, Y. Ronen, Y. Most, Y. Oreg, M. Heiblum, and H. Shtrikman, Nat. Phys. **8**, 887 (2012).
[14] M. T. Deng, C. L. Yu, G. Y. Huang, M. Larsson, P. Caroff, and H. Q. Xu, Nano Lett. **12**, 6414 (2012).
[15] V. Mourik, K. Zuo, S. M. Frolov, S. R. Plissard, E. P. A. M. Bakkers, and L. P. Kouwenhoven, Science **336**, 1003 (2012).
[16] S. M. Albrecht, A. P. Higginbotham, M. Madsen, F. Kuemmeth, T. S. Jespersen, J. Nygård, P. Krogstrup, and C. M. Marcus, Nature (London) **531**, 206 (2016).
[17] H. Zhang, Ö. Gül, S. Conesa-Boj, K. Zuo, V. Mourik, F. K. de Vries, J. van Veen, D. J. van Woerkom, M. P. Nowak, M. Wimmer, D. Car, S. Plissard, E. P. A. M. Bakkers, M. Quintero-Pérez, S. Goswami, K. Watanabe, T. Taniguchi, and L. P. Kouwenhoven, arXiv:1603.04069.
[18] A. Y. Kitaev, Phys. Usp. **44**, 131 (2001).
[19] R. M. Lutchyn, J. D. Sau, and S. D. Sarma, Phys. Rev. Lett. **105**, 077001 (2010).
[20] Y. Oreg, G. Refael, and F. von Oppen, Phys. Rev. Lett. **105**, 177002 (2010).
[21] A. Kitaev, Ann. Phys. (Amsterdam) **303**, 2 (2003).
[22] C. Nayak, S. H. Simon, A. Stern, M. Freedman, and S. Das Sarma, Rev. Mod. Phys. **80**, 1083 (2008).
[23] M. Kjaergaard, K. Wölms, and K. Flensberg, Phys. Rev. B **85**, 020503 (2012).
[24] G. L. Fatin, A. Matos-Abiague, B. Scharf, and I. Žutić, Phys. Rev. Lett. **117**, 077002 (2016).
[25] A. Matos-Abiague, J. Shabani, A. D. Kent, G. L. Fatin, B. Scharf, and I. Žutić, Solid State Commun. **262**, 1 (2017).
[26] I. Žutić, J. Fabian, and S. D. Sarma, Rev. Mod. Phys. **76**, 323 (2004).
[27] We measure the g factors in units of the Bohr magneton $\mu_B = (e\hbar/2m_0)$ and use the sign convention where the free electron g factor is $g_0 \approx +2$.
[28] C. R. Pidgeon, D. L. Mitchell, and R. N. Brown, Phys. Rev. **154**, 737 (1967).
[29] S. Vaitiekėnas, M. T. Deng, and C. M. Marcus (private communication).
[30] L. Landau and E. Lifshitz, *Course of Theoretical Physics* (Elsevier Science, New York, 1981).
[31] F. Kuemmeth, S. Ilani, D. C. Ralph, and P. L. McEuen, Nature (London) **452**, 448 (2008).
[32] E. A. Laird, F. Kuemmeth, G. A. Steele, K. Grove-Rasmussen, J. Nygård, K. Flensberg, and L. P. Kouwenhoven, Rev. Mod. Phys. **87**, 703 (2015).
[33] E. Kane, J. Phys. Chem. Solids **1**, 249 (1957).
[34] B. A. Foreman, Phys. Rev. B **56**, R12748 (1997).
[35] P. C. Sercel and K. J. Vahala, Phys. Rev. B **42**, 3690 (1990).
[36] K. J. Vahala and P. C. Sercel, Phys. Rev. Lett. **65**, 239 (1990).
[37] S. Çakmak, A. Babayev, E. Artunç, A. Kökçe, and S. Čakmaktepe, Physica (Amsterdam) **18E**, 365 (2003).
[38] See Supplemental Material at http://link.aps.org/supplemental/10.1103/PhysRevLett.119.037701, which includes additional Refs. [39–48] for a detailed description of the numerical simulations, discussion of the influence of the boundary conditions, and additional analytical and numerical results.
[39] F. Nichele, M. Kjaergaard, H. J. Suominen, R. Skolasinski, M. Wimmer, B.-M. Nguyen, A. A. Kiselev, W. Yi, M. Sokolich, M. J. Manfra, F. Qu, A. J. A. Beukman, L. P. Kouwenhoven, and C. M. Marcus, Phys. Rev. Lett. **118**, 016801 (2017).
[40] E. N. Bulgakov and A. F. Sadreev, J. Exp. Theor. Phys. Lett. **73**, 505 (2001).
[41] M. Graf and P. Vogl, Phys. Rev. B **51**, 4940 (1995).
[42] M. Tinkham, *Introduction to Superconductivity*, Dover Books on Physics Series (Dover Publications, New York, 1996).
[43] M. P. L. Sancho, J. M. L. Sancho, and J. Rubio, J. Phys. F **14**, 1205 (1984).
[44] M. P. L. Sancho, J. M. L. Sancho, and J. Rubio, J. Phys. F **15**, 851 (1985).
[45] M. Luisier, A. Schenk, W. Fichtner, and G. Klimeck, Phys. Rev. B **74**, 205323 (2006).
[46] S. Datta, *Electronic Transport in Mesoscopic Systems*, Cambridge Studies in Semiconductor Physics (Cambridge University Press, Cambridge, 1997).
[47] C. W. Groth, M. Wimmer, A. R. Akhmerov, and X. Waintal, New J. Phys. **16**, 063065 (2014).
[48] B. Scharf and I. Žutić, Phys. Rev. B **91**, 144505 (2015).

[49] L. C. L. Y. Voon, C. Galeriu, B. Lassen, M. Willatzen, and R. Melnik, Appl. Phys. Lett. **87**, 041906 (2005).
[50] Here j takes the role of s in the previous argument, as in these materials the p-type orbitals have nonzero local orbital angular momentum and are treated as spin-3/2 degrees of freedom.
[51] R. W. Robinett, Eur. J. Phys. **24**, 231 (2003).
[52] S. Tarucha, D. G. Austing, T. Honda, R. J. van der Hage, and L. P. Kouwenhoven, Phys. Rev. Lett. **77**, 3613 (1996).
[53] A. V. Rodina, A. Y. Alekseev, A. L. Efros, M. Rosen, and B. K. Meyer, Phys. Rev. B **65**, 125302 (2002).
[54] A. A. Mostofi, J. R. Yates, G. Pizzi, Y.-S. Lee, I. Souza, D. Vanderbilt, and N. Marzari, Comput. Phys. Commun. **185**, 2309 (2014).
[55] G. Kresse and J. Hafner, Phys. Rev. B **47**, 558 (1993).
[56] G. Kresse and J. Hafner, Phys. Rev. B **49**, 14251 (1994).
[57] G. Kresse and J. Furthmüller, Phys. Rev. B **54**, 11169 (1996).
[58] G. Kresse and J. Furthmüller, Comput. Mater. Sci. **6**, 15 (1996).
[59] P. E. Blöchl, Phys. Rev. B **50**, 17953 (1994).
[60] G. Kresse and D. Joubert, Phys. Rev. B **59**, 1758 (1999).
[61] Y.-S. Kim, K. Hummer, and G. Kresse, Phys. Rev. B **80**, 035203 (2009).
[62] J. Heyd, G. E. Scuseria, and M. Ernzerhof, J. Chem. Phys. **118**, 8207 (2003).
[63] J. Heyd and G. E. Scuseria, J. Chem. Phys. **121**, 1187 (2004).
[64] L. C. Lew Yan Voon, M. Willatzen, M. Cardona, and N. E. Christensen, Phys. Rev. B **53**, 10703 (1996).
[65] P. E. Faria, Jr., T. Campos, C. M. O. Bastos, M. Gmitra, J. Fabian, and G. M. Sipahi, Phys. Rev. B **93**, 235204 (2016).
[66] P. Krogstrup, N. L. B. Ziino, W. Chang, S. M. Albrecht, M. H. Madsen, E. Johnson, J. Nygård, C. M. Marcus, and T. S. Jespersen, Nat. Mater. **14**, 400 (2015).
[67] M. Gmitra and J. Fabian, Phys. Rev. B **94**, 165202 (2016).
[68] B. Nijholt and A. R. Akhmerov, Phys. Rev. B **93**, 235434 (2016).
[69] H. W. van Kesteren, E. C. Cosman, W. A. J. A. van der Poel, and C. T. Foxon, Phys. Rev. B **41**, 5283 (1990).
[70] P. Peyla, A. Wasiela, Y. Merle d'Aubigné, D. E. Ashenford, and B. Lunn, Phys. Rev. B **47**, 3783 (1993).
[71] W. Chang, S. M. Albrecht, T. S. Jespersen, F. Kuemmeth, P. Krogstrup, J. Nygård, and C. M. Marcus, Nat. Nanotechnol. **10**, 232 (2015).
[72] Our simulations do not include the renormalization effects of the superconductor [73,74], which could lead to a reduction of the resulting g factor.
[73] T. D. Stanescu, R. M. Lutchyn, and S. D. Sarma, Phys. Rev. B **84**, 144522 (2011).
[74] D. Sticlet, B. Nijholt, and A. Akhmerov, Phys. Rev. B **95**, 115421 (2017).